Heliyon

ELSEVIER

Received:
26 June 2017
Revised:
15 September 2017
Accepted:
8 November 2017

Cite as: Edward Shitsi, Seth Kofi Debrah, Vincent Yao Agbodemegbe, Emmanuel Ampomah-Amoako. Numerical investigation of heat transfer in parallel channels with water at supercritical pressure. Heliyon 3 (2017) e00453.
doi: 10.1016/j.heliyon.2017.e00453

Numerical investigation of heat transfer in parallel channels with water at supercritical pressure

Edward Shitsi *, Seth Kofi Debrah, Vincent Yao Agbodemegbe, Emmanuel Ampomah-Amoako

Department of Nuclear Engineering, School of Nuclear and Allied Sciences, University of Ghana, P.O. Box AE 1, Atomic Energy, Kwabenya, Accra, Ghana

* Corresponding author.
E-mail address: edwardshitsi@yahoo.com (E. Shitsi).

Abstract

Thermal phenomena such as heat transfer enhancement, heat transfer deterioration, and flow instability observed at supercritical pressures as a result of fluid property variations have the potential to affect the safety of design and operation of Supercritical Water-cooled Reactor SCWR, and also challenge the capabilities of both heat transfer correlations and Computational Fluid Dynamics CFD physical models. These phenomena observed at supercritical pressures need to be thoroughly investigated.

An experimental study was carried out by Xi to investigate flow instability in parallel channels at supercritical pressures under different mass flow rates, pressures, and axial power shapes. Experimental data on flow instability at inlet of the heated channels were obtained but no heat transfer data along the axial length was obtained. This numerical study used 3D numerical tool STAR-CCM+ to investigate heat transfer at supercritical pressures along the axial lengths of the parallel channels with water ahead of experimental data. Homogeneous axial power shape HAPS was adopted and the heating powers adopted in this work were below the experimental threshold heating powers obtained for HAPS by Xi. The results show that the Fluid Centre-line Temperature FCLT increased linearly below and above the PCT region, but flattened at the PCT region for all the system

http://dx.doi.org/10.1016/j.heliyon.2017.e00453

parameters considered. The inlet temperature, heating power, pressure, gravity and mass flow rate have effects on WT (wall temperature) values in the NHT (normal heat transfer), EHT (enhanced heat transfer), DHT (deteriorated heat transfer) and recovery from DHT regions. While variation of all other system parameters in the EHT and PCT regions showed no significant difference in the WT and FCLT values respectively, the WT and FCLT values respectively increased with pressure in these regions. For most of the system parameters considered, the FCLT and WT values obtained in the two channels were nearly the same. The numerical study was not quantitatively compared with experimental data along the axial lengths of the parallel channels, but it was observed that the numerical tool STAR-CCM+ adopted was able to capture the trends for NHT, EHT, DHT and recovery from DHT regions. The heating powers used for the various simulations were below the experimentally observed threshold heating powers, but heat transfer deterioration HTD was observed, confirming the previous finding that HTD could occur before the occurrence of unstable behavior at supercritical pressures. For purposes of comparing the results of numerical simulations with experimental data, the heat transfer data on temperature oscillations obtained at the outlet of the heated channels and instability boundary results obtained at the inlet of the heated channels were compared. The numerical results obtained quite well agree with the experimental data. This work calls for provision of experimental data on heat transfer in parallel channels at supercritical pressures for validation of similar numerical studies.

Keywords: Mechanical engineering, Nuclear engineering

1. Introduction

Experimental and numerical research activities are ongoing worldwide to develop Gen IV reactors to be built in the near future. With growing demand for energy, it becomes necessary to improve Energy Sustainability, Economics, Safety and reliability, and Proliferation resistance and physical protection of nuclear energy systems. Gen IV reactors were selected by the Generation IV International Forum (GIF) to achieve these purposes. Energy Sustainability focuses on sustainability of energy generation, ensuring long-term availability of nuclear fuel, and by effective nuclear fuel utilization and minimization of waste. Economics focuses on competitiveness of nuclear energy in terms of production cost, financial risk and life cycle cost compared to other energy sources. Safety and reliability focuses on the reactor type having very low chances of experiencing core damage, and there must not be the need for on-site emergency response. Proliferation resistance and physical protection focuses on the reactor type being a very unattractive route for diversion or theft of weapons-usable materials, and preventing terrorist acts by providing increased physical protection (GIF, 2002; Chaudri et al., 2013).

http://dx.doi.org/10.1016/j.heliyon.2017.e00453

A theoretical nuclear power plant cooled and moderated with supercritical water termed SCWR, one of the Gen IV reactors, is under study with the purpose to achieve a high thermal efficiency, improve safety and economic competitiveness compared to existing Light Water Reactors LWRs. In fact, SCWR is a logical extension of existing Pressurized Water Reactor (PWR) and Boiling Water Reactor (BWR) combined with the existing technology of super-critical water cooled fossil fuel fired power plants. The most typical designs include Supercritical Light Water Reactor (Super LWR) and Supercritical Water-cooled Fast Reactor (SWFR) in Japan, High Performance Light Water Reactor (HPLWR) in Europe, CANDU-SCWR in Canada, American SCWR in the USA and SCWR with mixed spectrum core (SCWR-M) in China (IAEA-TECDOC-1746, 2014; Zhao et al., 2014).

Research to understand and predict fluid flow and heat transfer at supercritical pressures is a major concern of nuclear engineers worldwide because of drastic variations in fluid properties at the vicinity of pseudo-critical temperature (Shitsi et al., 2017). These variations in fluid properties, coolant inlet temperature range (250–280 °C) and coolant exit temperature range (500–625 °C) among other factors of SCWR operated at supercritical pressures are likely to produce heat transfer characteristics different from that obtained at sub-critical pressures. Critical point of water is associated with critical temperature of 374.0 °C and critical pressure of 22.1 MPa. The general purpose of heat transfer research at supercritical pressures is to provide information and data; heat transfer correlations and other physical models; and numerical tools for the design of heat transfer equipment, licensing heat transfer facilities and safety assessment of operation of heat transfer facilities.

Yang et al., 2007 carried out numerical investigation of heat transfer in upward flows of supercritical water in circular tubes and tight fuel rod bundles using the commercial CFD code STAR-CD 3.24. Adopting the three-dimensional (3-D) tool STAR-CD 3.24, simulations were performed in flow-channels of the two main lattices such as square lattice and triangular lattice fuel rod bundles. The turbulence models including the two-layer model (Hassid and Poreh) and standard k–ε high Re model performed better in predicting heat transfer at supercritical pressures than the other models that were assessed. A strong non-uniformity of the circumferential distribution of temperature at the cladding surface in the square lattice bundle with a small pitch-to-diameter ratio (P/D) was also observed. This phenomenon was not observed in the triangular lattice bundle with a small P/D. Sharabi et al., 2008 and Sharabi, 2008 reported cyclic occurrence of heat transfer deterioration and restoration during flow oscillations in heated channels with supercritical fluids. They mentioned that it was not certain whether spacer grids in reactor core configurations could generate turbulence which would prevent the occurrence of heat transfer deterioration HTD. HTD was also predicted to occur before the occurrence of unstable behavior at supercritical pressures. Wang et al., 2014 and

http://dx.doi.org/10.1016/j.heliyon.2017.e00453

Wang et al., 2016 carried out an experimental investigation of heat transfer at supercritical pressure in a 2 × 2 rod bundle with water. Influences of the parameters including heat flux, system pressure and mass flux on heat transfer were examined. The maximum and minimum wall temperatures were observed respectively at the surface facing the corner gap between the heated rod and the ceramic tube, and at the surface facing the center sub-channel. The difference between maximum and minimum wall temperatures was found to be dependent on the heat flux or mass flux. The bulk temperature distribution through the flow cross-section was not uniform, and temperature variation became small as the bulk temperature approached the pseudo-critical temperature. Some selected heat transfer correlations developed for supercritical water were assessed against the test data. Prediction of the Jackson correlation most closely predicted the test data. Zhang et al., 2014 numerically investigated heat transfer of supercritical fluid, Freon R12, in a 7-rod bundle. Some selected turbulent models were assessed for predicting the heat transfer performance of Freon R12 through the rod bundle. The turbulence models performed well in predicting the experimental data in the normal heat transfer region. The ω type turbulence models performed better in predicting heat transfer quantitatively in the deteriorated heat transfer region near the critical region. Strong non-uniform circumferential temperature distribution near the pseudo-critical temperature region was also observed.

Gu et al., 2015a and Gu et al., 2015b performed experimental studies to investigate heat transfer to supercritical water in a 2 × 2 rod bundle with two channels. Water flowed downward in the first channel and then flowed upward in the second channel to cool the rod bundle. Results of their studies showed that heat transfer behavior inside the rod bundle was similar to those observed in tube or annuli. Jackson and Fewster, and Bishop et al. correlations gave the best predictions when compared with the experimental data among some selected heat transfer correlations that were tested and evaluated. Gu et al., 2016 performed similar experimental studies on heat transfer to supercritical water in the 2 × 2 rod bundle with two channels. The rod bundle was wrapped with wires to produce mixing effect on heat transfer. Deterioration in heat transfer and significant non-uniformity of circumferential wall-temperature distribution around the heater rods were observed in the bundle. There was significant reduction in heat transfer deterioration due to the mixing effects produced by the wire wraps. The enhancement in heat transfer due to the presence of wire wraps became obvious under a high mass flux condition. Huang et al., 2016 carried out a review of heat transfer at supercritical pressures involving some selected fluids such as water, carbon dioxide and hydrocarbon fuels flowing in smooth and enhanced tubes. They found out that heat transfer in enhanced tubes was much better than that in smooth tubes. Rahman et al., 2016 reviewed studies on supercritical water heat transfer with the aim of providing references for SCWR researchers. It was found out that

http://dx.doi.org/10.1016/j.heliyon.2017.e00453

most of the CFD studies and experimental studies were performed with single tube geometry due to the complexity of parallel channel geometry. Because of studies performed with parallel channel geometry could provide detailed information to the design of the SCWR core, they called for more studies in parallel channel geometry at supercritical pressures in the future. Xi (Xi et al., 2014a) and Shitsi et al., 2017 respectively carried out experimental and numerical studies and investigated flow instability in parallel channels at supercritical pressures under different mass flow rates, pressures, and axial power shapes. Experimental and numerical data on flow instability at inlet of the heated channels were obtained but no heat transfer data along the axial length was obtained. The objective of this work is to address heat transfer in parallel channels with water at supercritical pressure. The capability of the numerical tool STAR-CCM+ adopted to capture the trends for Normal heat transfer (NHT), Improved or Enhanced heat transfer (IHT or EHT), Deteriorated heat transfer (DHT) and recovery from DHT regions is investigated along the flow channel. NHT is characterised with wall heat transfer coefficients or wall temperatures similar to those observed at subcritical convective heat transfer far from the critical or pseudo-critical region. In NHT regime, the bulk fluid temperature or the fluid centre-line temperature FCLT is below the pseudo-critical temperature. IHT or EHT is characterised with higher values of the wall heat transfer coefficient or low values of wall temperature. The IHT or EHT regime is observed near the critical or pseudo-critical point. DHT is characterised with lower values of the wall heat transfer coefficient or higher values of wall temperature. The DHT regime is observed when the wall temperature is greater than the pseudo-critical temperature and the bulk temperature or the FCLT is less than the pseudo-critical temperature. Effects of parameters such as heating power (or heat flux), mass flow rate, inlet temperature, gravity and pressure on supercritical heat transfer are discussed based on obtained wall temperatures WTs and fluid centre-line temperatures FCLTs.

2. Theory

2.1. Reference experimental setup and adopted 3D geometry

The geometry adopted by Xi (Xi et al., 2014a) in investigating flow instability at supercritical pressures is adopted in this study. Only the fluid region was considered. Xi performed a flow instability experiment in parallel channels with supercritical water in Nuclear Power Institute of China (NPIC). Influences of parameters such as system pressures, inlet mass flow rates, inlet temperatures and axial power shapes on flow instability were investigated. The STAR-CCM+ 3-D mesh of the geometrical model and the Wall mesh adopted by Shitsi et al., 2017 were also adopted in this work. Schematic diagrams of experimental test facility, the test section and INCONEL 625 pipe used for the parallel channels in the test section are presented in the numerical study carried out by Shitsi et al., 2017. The

http://dx.doi.org/10.1016/j.heliyon.2017.e00453

test section of the geometrical model consists of two parallel channels with inner diameter 6 mm, outer diameter 19 mm and heated length of 3105 mm. The total mesh size with 1.0 mm base size and 7 prism layers of the two tee bends, four diffusers and 2 heated parallel channels is approximately 2997000. Different mesh sizes have been examined before deciding on the optimum mesh size of 2997000 cells to save computational time. Polyhedral Mesher, Prism Layer Mesher and Surface Remesher were selected for the meshing. Half of the full geometry (symmetrical boundary condition) was used in order to save computational time. Non-Slip wall boundary condition was adopted at the wall. Adiabatic boundary condition was adopted for the non-heated walls and heat flux boundary condition was adopted for the heated walls of the parallel channels. Mass flow rate inlet and pressure outlet boundary conditions were adopted for the inlet and outlet respectively. The heating powers applied in the experiment are net heating powers applied to the fluid region. The heat loss had been taken care off in the experiment. The numerical simulation considered only the fluid region and the net heating powers were applied to the fluid region too for the numerical simulations. The focus of the study is not on effects of heating structures where the thickness of the pipe has to be taken into consideration. Detailed information on the experimental facility and the flow instability experiment can be found in Xi et al., 2014a.

To ensure that the inlet and outlet pressure loss coefficients employed in the experiment and numerical simulation are the same, the pressure jump model was used in the numerical simulation to adjust the inlet and outlet pressure loss coefficients. The inlet and outlet pressure loss coefficient used in the experiment are:

$K_{in1} = 4.1$, $K_{in2} = 4.3$; and $K_{out1} = 3.9$, $K_{out2} = 3.8$

2.2. Physical models

Mass conservation equation (Equation (1)):

$$\frac{\partial \rho}{\partial t} + \nabla.(\rho u) = 0 \tag{1}$$

U- Momentum equation (Equation (2)):

$$\frac{\partial(\rho u)}{\partial t} + div(\rho u\, u) = div(ugradu) - \frac{\partial P}{\partial x} + \left[-\frac{\partial(\rho \overline{u'^2})}{\partial x} - \frac{\partial(\rho \overline{u'v'})}{\partial y} - \frac{\partial(\rho \overline{u'w'})}{\partial z} \right] + S_u \tag{2}$$

http://dx.doi.org/10.1016/j.heliyon.2017.e00453

V- Momentum equation (Equation (3)):

$$\frac{\partial(\rho v)}{\partial t} + div(\rho v\, u) = div(ugradv) - \frac{\partial P}{\partial y} + \left[-\frac{\partial(\rho\overline{u'v'})}{\partial x} - \frac{\partial(\rho\overline{v'^2})}{\partial y} - \frac{\partial(\rho\overline{v'w'})}{\partial z}\right] + S_v \tag{3}$$

W- Momentum equation (Equation (4)):

$$\frac{\partial(\rho w)}{\partial t} + div(\rho w\, u) = div(ugradw) - \frac{\partial P}{\partial z} + \left[-\frac{\partial(\rho\overline{u'w'})}{\partial x} - \frac{\partial(\rho\overline{w'v'})}{\partial y} - \frac{\partial(\rho\overline{w'^2})}{\partial z}\right] + S_w \tag{4}$$

Energy conservation equation (Equation (5)):

$$\frac{\partial(\rho T)}{\partial t} + div(\rho\, u\, T) = div\left(\frac{\lambda}{C_p} gradT\right) + \left[-\frac{\partial(\rho\overline{u'T'})}{\partial x} - \frac{\partial(\rho\overline{v'T'})}{\partial y} - \frac{\partial(\rho\overline{w'T'})}{\partial z}\right] + S_T \tag{5}$$

where the symbols have their usual meanings (Xi et al., 2014b; Versteeg and Malalasekera, 1995).

Three different turbulence models were tested for their capability of capturing the trends for NHT, EHT, DHT regions; and also for their capability of capturing the trend for recovery from DHT region in parallel channels with water at supercritical pressures. These turbulence models include Standard Low Reynolds Number k-ε model (LIEN), Standard k–ε model and k-ω SST model (Cd-Adapco, 2015). The all y^+ wall treatment is adopted for LIEN, and high- y+ wall treatment is adopted for Standard k–ε model and k-ω SST model.

The turbulence kinetic energy and dissipation rate equations (Equations (6) and (7)) to be solved in Standard Low Reynolds Number k-ε model (LIEN) are respectively described as:

$$\frac{\partial(\rho k)}{\partial t} + \frac{\partial\left(\rho k u_j\right)}{\partial x_j} = \frac{\partial}{\partial x_j}\left[\left(\mu + \frac{\mu_t}{\delta_k}\right)\frac{\partial k}{\partial x_j}\right] + G_k + G_b - \rho\varepsilon + S_k \tag{6}$$

$$\frac{\partial(\rho\varepsilon)}{\partial t} + \frac{\partial\left(\rho\varepsilon u_j\right)}{\partial x_j} = \frac{\partial}{\partial x_j}\left[\left(\mu + \frac{\mu_t}{\delta_\varepsilon}\right)\frac{\partial \varepsilon}{\partial x_j}\right] + C_{1\varepsilon} f_1 \frac{\varepsilon}{k}(G_k + G_b) - C_{2\varepsilon} f_2 \rho\frac{\varepsilon^2}{k} + S_\varepsilon \tag{7}$$

The turbulence kinetic energy and dissipation rate equations (Equations (8) and (9) to be solved in standard k-ε model are respectively described as:

$$\frac{\partial(\rho k)}{\partial t} + \frac{\partial\left(\rho k u_j\right)}{\partial x_j} = \frac{\partial}{\partial x_j}\left[\left(\mu + \frac{\mu_t}{\delta_k}\right)\frac{\partial k}{\partial x_j}\right] + G_k + G_b - \rho\varepsilon - Y_M + S_k \tag{8}$$

http://dx.doi.org/10.1016/j.heliyon.2017.e00453

$$\frac{\partial(\rho\varepsilon)}{\partial t}+\frac{\partial\left(\rho\varepsilon u_j\right)}{\partial x_j}=\frac{\partial}{\partial x_j}\left[\left(\mu+\frac{\mu_t}{\delta_\varepsilon}\right)\frac{\partial\varepsilon}{\partial x_j}\right]+C_{1\varepsilon}\frac{\varepsilon}{k}(G_k+C_{3\varepsilon}G_b)-C_{2\varepsilon}\rho\frac{\varepsilon^2}{k}+S_\varepsilon \tag{9}$$

The turbulence kinetic energy and specific dissipation rate equations (Equations (10) and (11)) to be solved in k-ω SST model are respectively described as:

$$\frac{\partial(\rho k)}{\partial t}+\frac{\partial\left(\rho k u_j\right)}{\partial x_j}=\frac{\partial}{\partial x_j}\left[\left(\mu+\frac{\mu_t}{\delta_k}\right)\frac{\partial k}{\partial x_j}\right]+G_k+G_b-Y_k+S_k \tag{10}$$

$$\partial\frac{\rho\omega}{\partial t}+\partial\frac{\rho\omega u_j}{\partial x_j}=\frac{\partial}{\partial x_j}\mu+\frac{\mu_t\partial\omega}{\delta_\omega\partial x_j}]+G_\omega+D_\omega-Y_\omega+S_\omega \tag{11}$$

Equations (12) (13) (14) are definitions of some constants in Equations (6)–(11).

$$\sigma_k=1;\sigma_\varepsilon=1.2;C_{1\varepsilon}=1.44;C_2=1.9;C_{3\varepsilon}=tan|\frac{w_{//g}}{w_{\perp g}}| \tag{12}$$

$$C_1=max\left[0.43,\frac{\eta}{\eta+5}\right];\eta=S\frac{k}{\varepsilon};S=\sqrt{2S_{ij}S_{ij}} \tag{13}$$

$$f_1=1.0;f_2=1-0.3exp\left(-Re_t{}^2\right);Re_t=\frac{\rho k^2}{\mu\varepsilon} \tag{14}$$

where the terms: S_k, S_ε, and S_ω are user-specified source terms; $C_{1\varepsilon}$, $C_{2\varepsilon}$, $C_{3\varepsilon}$, C_1 and C_2 are constants (turbulence model coefficients); G_k (turbulent production), G_b (buoyancy production), G_ω (production of ω), Y_M (Compressibility Modification), μ_t (turbulent viscosity), D_ω (Cross-Derivation), Y_ω (dissipation of ω due to turbulence) and f1, f2 (damping functions) are obtained from additional equations associated with respective models (Cd-Adapco, 2015; Xi et al., 2014b). The other undefined terms have their usual meanings.

As in many other available CFD codes, STAR-CCM+ makes use of finite volume discretization technique to discretize the equations. The method of discretization is beyond the scope of the work.

3. Results

3.1. Turbulence models consideration

There are several studies that obtained the finding, turbulence model adopted in 3D numerical studies, has significant effect on the performance of a numerical tool used to predict heat transfer in fluid flow and heat transfer systems (Cheng et al., 2007; Yang et al., 2007; Wen and Gu, 2010; Angelucci et al., 2013; Liu et al., 2013; Zhang et al., 2014). Three turbulence models, namely, k-ω SST, LIEN and Standard k-ε were tested for their capability of capturing the trends for NHT, EHT, DHT regions; and also for their capability of capturing the trend for recovery from DHT region in parallel channels with water at supercritical pressures. Implicit formulation and time step of 0.01 s were adopted. Segregated flow approach was

http://dx.doi.org/10.1016/j.heliyon.2017.e00453

adopted to solve the governing equations. The simulations carried in this work are 3-D unsteady state simulations. NIST Table (NIST, 2002) was used to calculate physical properties of water.

Fig. 1 and Fig. 2 respectively show performance of the three turbulence models TMs in capturing heat transfer at system pressures of 23 MPa (with pseudo-critical temperature PCT of 377.5 °C) and 25 MPa (with PCT of 384.9 °C), 125 kg/h mass flow rate, 200 °C inlet temperature and 72 kW total heating power for the two channels. Uniform axial power shape, where constant heat flux or heating power is applied to the heated sections of the parallel channels, was adopted for all the numerical simulations. Influence of gravity on heat transfer HT was taken into consideration in all the simulations, unless it was stated otherwise. At 23 MPa, the three TMs produced nearly the same trend and values for fluid centre-line temperature FCLT. The three TMs produced similar trends for NHT up to 390 °C wall temperature WT, produced nearly the same trend and values in the EHT region near the 390 °C WT located at 1.1 m length of the heated axial length of 3.105 m. LIEN and Standard k-ε TMs developed sharp rise in the WT (DHT region) up to 600 °C for LIEN and 690 °C for Standard k-ε. DHT region was also observed for k-ω SST model up to WT of 600 °C. The enhancement in HT was observed again after DHT region for all the three TMs (recovery from DHT region), but k-ω SST produced large WT values than LIEN and Standard k-ε TMs towards the end of the heated length. The WT values towards the end of the axial

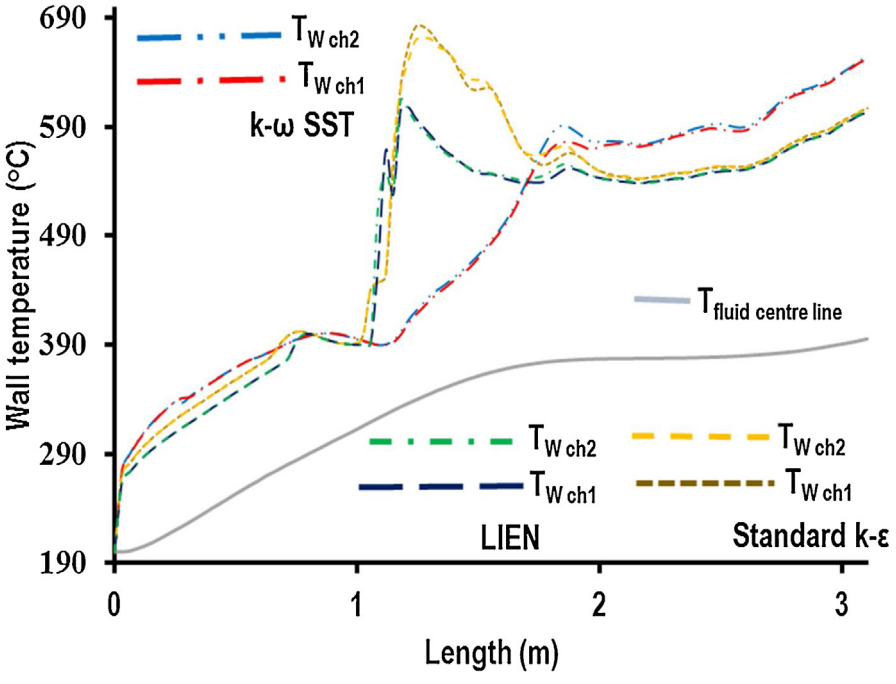

Fig. 1. Performance of turbulence models at 23 MPa.

http://dx.doi.org/10.1016/j.heliyon.2017.e00453

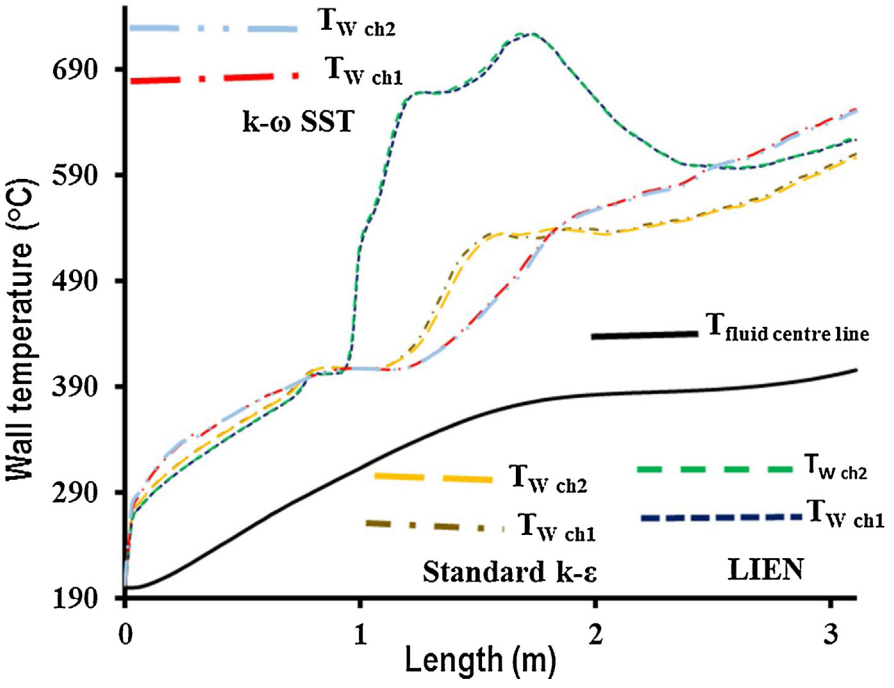

Fig. 2. Performance of turbulence models at 25 MPa.

length were nearly the same for LIEN and Standard k-ε TMs. The FCLT and WT values produced by the TMs in each of the two channels were nearly the same for both system pressures of 23 MPa and 25 MPa. The trends for WT and FCLT values observed for NHT, EHT, DHT and recovery from DHT regions for the three TMs at 25 MPa were similar to those obtained at 23 MPa. But only LIEN produced sharp rise of WT values in the DHT region at 25 MPa. The enhancement in HT after DHT region was remarkable for both Standard k-ε and LIEN TMs compared to that of k-ω SST model at 23 MPa (recovery from DHT region). The enhancement in HT after DHT region was remarkable for only LIEN compared to that of Standard k-ε and k-ω SST TMs at 25 MPa (recovery from DHT region). There were no significant differences in the WT values produced in the NHT and EHT regions by the three TMs at 23 MPa and 25 MPa. The significant differences in the WT values produced by the TMs occurred in the DHT region. In fact, the TMs produced nearly the same values of FCLT at both 23 MPa and 25 MPa. To my best of knowledge, there is no experimental data available on HT in parallel channels at supercritical pressures for comparison of the numerical simulations. k-ω SST TM was used to obtain results for all the numerical simulations because it was widely reported in literature to perform better than other TMs in most cases (Wen and Gu, 2010; Angelucci et al., 2013, Liu et al., 2013; Zhang et al., 2014).

http://dx.doi.org/10.1016/j.heliyon.2017.e00453

3.2. Influence of pressure on heat transfer

Fig. 3 and Fig. 4 respectively show the effects of system pressures 23 MPa and 25 MPa on HT at both 125 kg/h and 145 kg/h mass flow rates, 200 °C inlet temperature and total heating power of 72 kW for the two heated channels. For both 125 kg/h and 145 kg/h, the trend of values for the FCLT behaved nearly the same for the two system pressures, but the values for 25 MPa were larger than that of 23 MPa at the PCT region and after the PCT region. The trend for the FCLT increased linearly but flattened at the PCT region for both mass flow rates. The finding for FCLT was similar to experimental finding obtained by Wang et al., 2014; Wang et al., 2016; Gu et al., 2015a; Gu et al., 2015b and Gu et al., 2016 for bulk fluid temperatures that were analyzed for different system pressures in rod bundle geometry. NHT, EHT, DHT and recovery from the DHT regions were observed for the WT values at both system pressures. Pressure had no influence on WT values in the NHT region at both 125 kg/h and 145 kg/h. The WT values increased with pressure for both mass flow rates in the EHT region. The WT values in the DHT region at 23 MPa were larger than that at 25 MPa, but the variations in the WT values in the recovery from DHT region were not significant for both system pressures at 125 kg/h and 145 kg/h. The FCLT and WT values were nearly the same in each of the heated channels for both system pressures operated at 125 kg/h and 145 kg/h except the WT values in channel 1 were larger than that of channel 2 in the DHT and recovery from DHT regions at 145 kg/h.

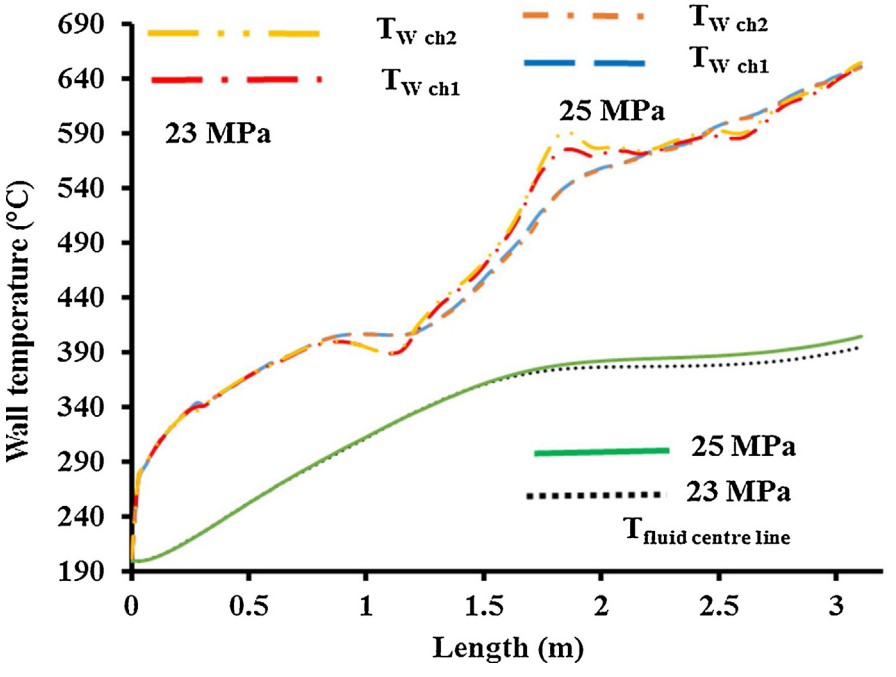

Fig. 3. Influence of system pressure on HT at 125 kg/h.

http://dx.doi.org/10.1016/j.heliyon.2017.e00453

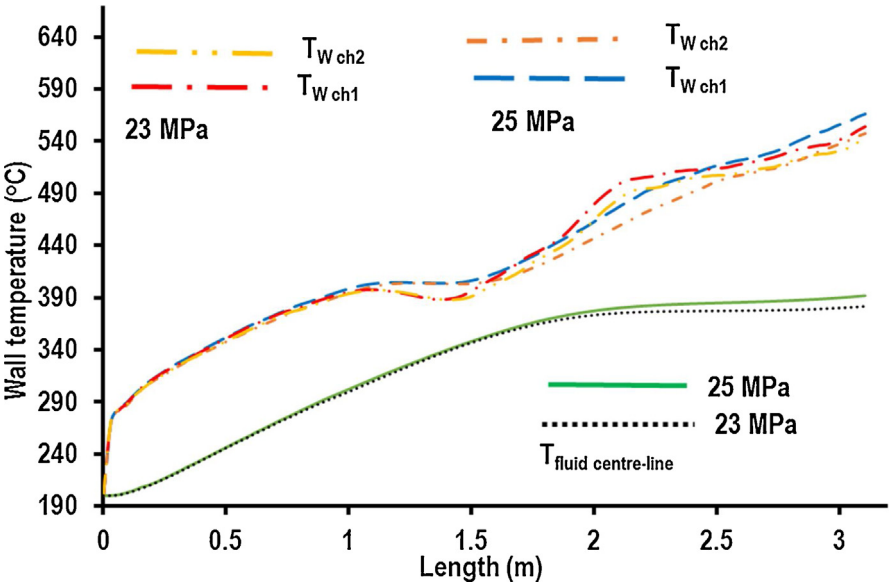

Fig. 4. Influence of system pressure on HT at 145 kg/h.

3.3. Influence of heating power/heat flux on heat transfer

Fig. 5 and Fig. 6 show respectively the results for influences of heating power on HT at 200 °C inlet temperature and 125 kg/h mass flow rate for both 23 MPa and 25 MPa. The total heating powers compared include 72 kW (36 kW/1230.1831 kW/m^2, for each channel); 68 kW (34 kW/1161.8396 kW/m^2, for each channel);

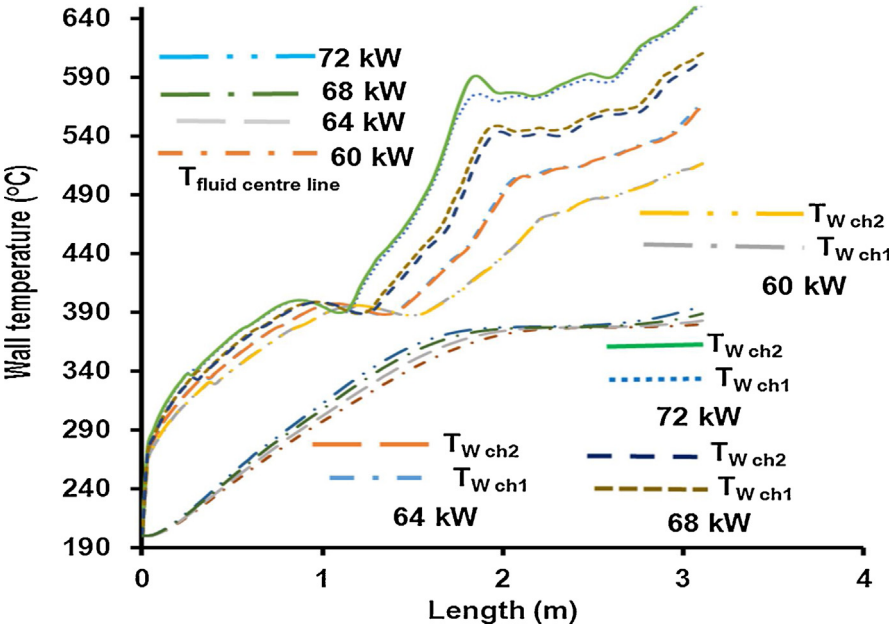

Fig. 5. Influence of heat flux on HT at 23 MPa.

http://dx.doi.org/10.1016/j.heliyon.2017.e00453

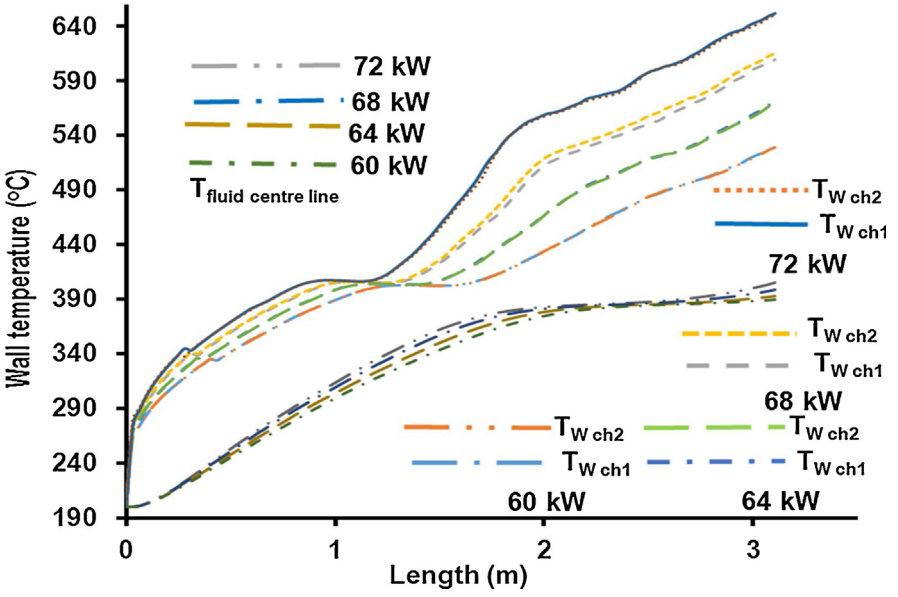

Fig. 6. Influence of heat flux on HT at 25 MPa.

64 kW (32 kW/1093.4961 kW/m^2, for each channel); and 60 kW (30 kW/1025.1526 kW/m^2, for each channel). At 23 MPa, NHT, EHT, DHT and recovery from DHT regions were observed for all the heating powers compared, the largest WT values were produced by 72 kW, and the lowest values of the WT were produced by 60 kW. At 25 MPa, the trends of NHT, EHT, DHT and recovery from DHT regions for WT values were similar to that obtained for 23 MPa. At both system pressures, the WT values in the EHT region were nearly the same for all the heating powers compared. The FCLT values increased with the heating power except at the PCT region where the values were nearly equal. The trend for FCLT values increased linearly up to the PCT region, flattened at the PCT region (i.e., the values were nearly the same and equal to PCT), and increased thereafter along the axial length. There were no significant differences between the FCLT and WT values with increase of heating power in each of the heated channels at both system pressures for the heating powers compared.

3.4. Influence of mass flow rate on heat transfer

Fig. 7 and Fig. 8 respectively show the results for the influences of system mass flow rates 125 kg/h and 145 kg/h on HT at 72 kW heating power and 200 °C inlet temperature for both system pressures of 23 MPa and 25 MPa. At both 23 MPa and 25 MPa, the trends of WT values obtained for NHT, DHT and recovery from DHT regions for the two system mass flow rates were similar, but the WT values for 125 kg/h were larger than that of 145 kg/h. The WT values in the EHT regions were nearly the same for both system mass flow rates at 23 MPa and 25 MPa. The FCLT values increased linearly below and above the PCT region, but flattened at the PCT

http://dx.doi.org/10.1016/j.heliyon.2017.e00453

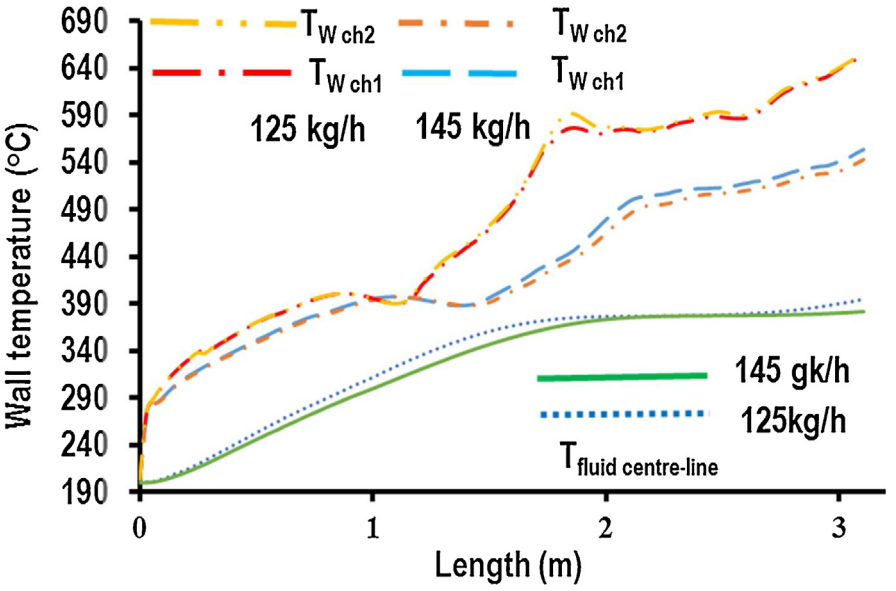

Fig. 7. Influence of Mass flow rate on HT at 23 MPa.

region. The FCLT values at 125 kg/h were larger than that at 145 kg/h but the FCLT values were nearly the same at the PCT region for both mass flow rates. The FCLT values in channels 1 and 2 were nearly the same with increase of mass flow rate. For both system mass flow rates of 125 kg/h and 145 kg/h at 23 MPa and 25 MPa, the WT values in each of the two channels were nearly the same except the

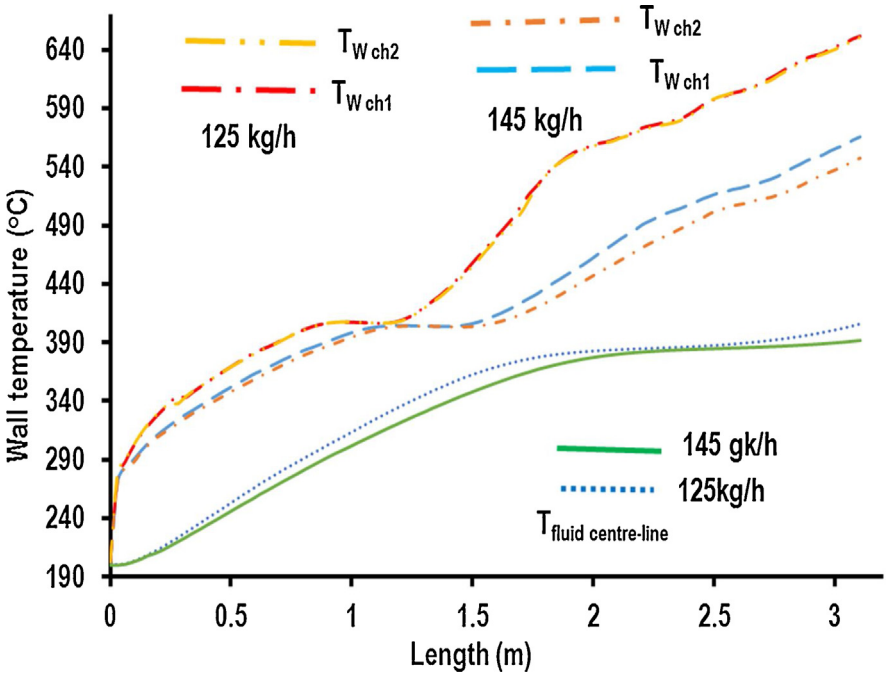

Fig. 8. Influence of Mass flow rate on HT at 25 MPa.

http://dx.doi.org/10.1016/j.heliyon.2017.e00453

WT values in channel 1 were larger than that in channel 2 for 145 kg/h in the DHT and recovery from DHT regions.

3.5. Influence of inlet temperature on heat transfer

Fig. 9 and Fig. 10 respectively show influences of inlet temperatures (200 °C, 250 °C and 300 °C) on HT at 72 kW heating power and 125 kg/h for system pressures of 23 MPa and 25 MPa. At 23 MPa, the FCLT values increased linearly below and above the PCT region, but flattened at the PCT region. The FCLT values were nearly the same for both channels 1 and 2. The largest FCLT values were obtained for 300 °C and lowest FCLT values were obtained for 200 °C but the FCLT values were nearly the same at the PCT region for all the inlet temperatures compared. The trends of WT values for NHT, EHT, DHT and recovery from DHT regions were similar for the inlet temperatures compared, but the largest WT values were produced by 300 °C and lowest WT values were produced by 200 °C. The WT values were nearly the same in the EHT regions just before and after the DHT region for all the inlet temperatures compared at 23 MPa. The differences in WT values for channels 1 and 2 were not significant but became obvious with increase in the inlet temperature in the DHT and recovery from DHT regions. At 25 MPa, the trends for FCLT and WT values were similar to that obtained at 23 MPa, but the differences in WT values for channels 1 and 2 became obvious only for 250 °C

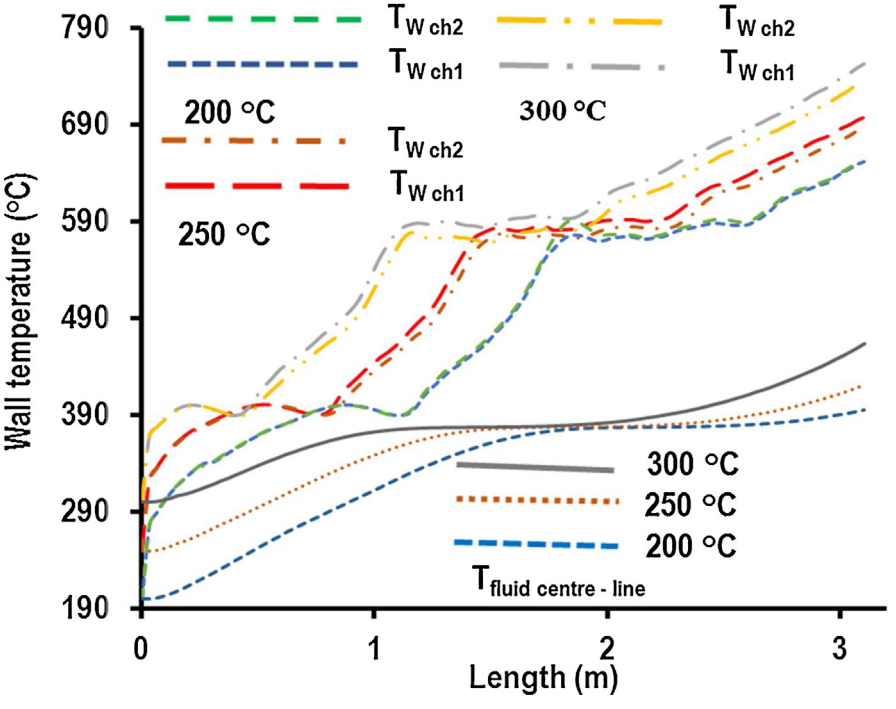

Fig. 9. Influence of inlet temperature on HT at 23 MPa.

http://dx.doi.org/10.1016/j.heliyon.2017.e00453

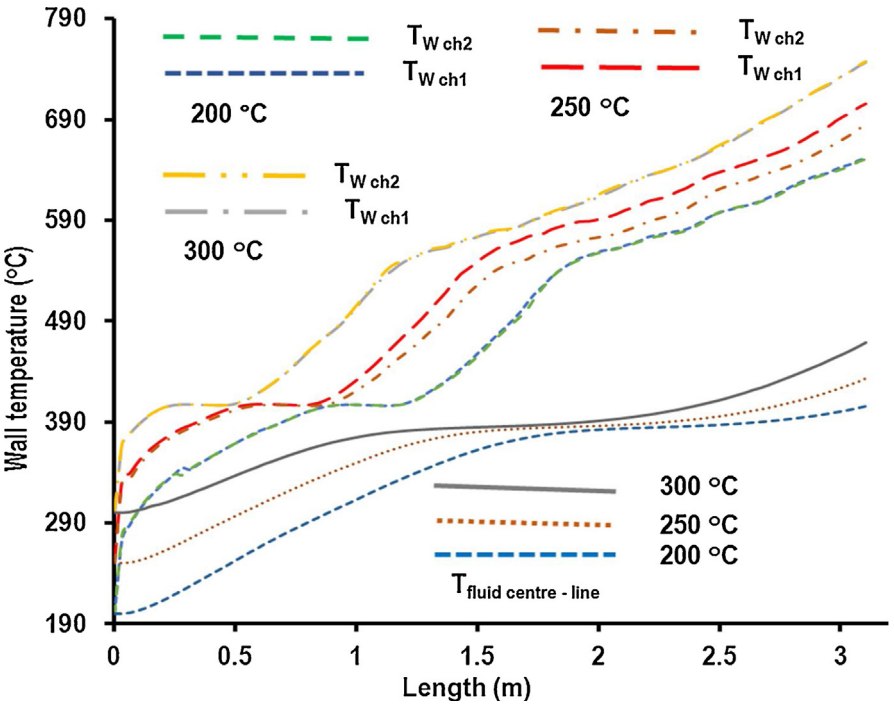

Fig. 10. Influence of inlet temperature on HT at 25 MPa.

inlet temperature in the DHT and recovery from DHT regions, and also the WT values increased with inlet temperature after the DHT region at 25 MPa.

3.6. Influence of gravity on heat transfer

Fig. 11 and Fig. 12 show influences of gravity on HT at 125 kg/h, 72 kW heating power and 200 °C inlet temperature for system pressures 23 MPa and 25 MPa respectively. At both 23 MPa and 25 MPa, nearly the same trends and WT values for NHT, EHT, DHT and recovery from DHT regions were obtained for the two systems with or without gravity influence except the WT values for system without gravity influence were larger than that of system with gravity influence in the DHT region at 23 MPa. The trends and values for the FCLT obtained for the two systems were nearly equal. The FCLT values increased linearly below and above the PCT region, but flattened at the PCT region. The FCLT and WT values for each of the two channels were nearly the same for the system operated with or without gravity influence.

3.7. Comparison between numerical simulation and experiment

For purposes of comparing the results of numerical simulations with experimental data, heat transfer data on temperature oscillations obtained at the outlet of the heated channels and instability boundary results obtained at the inlet of the heated

http://dx.doi.org/10.1016/j.heliyon.2017.e00453

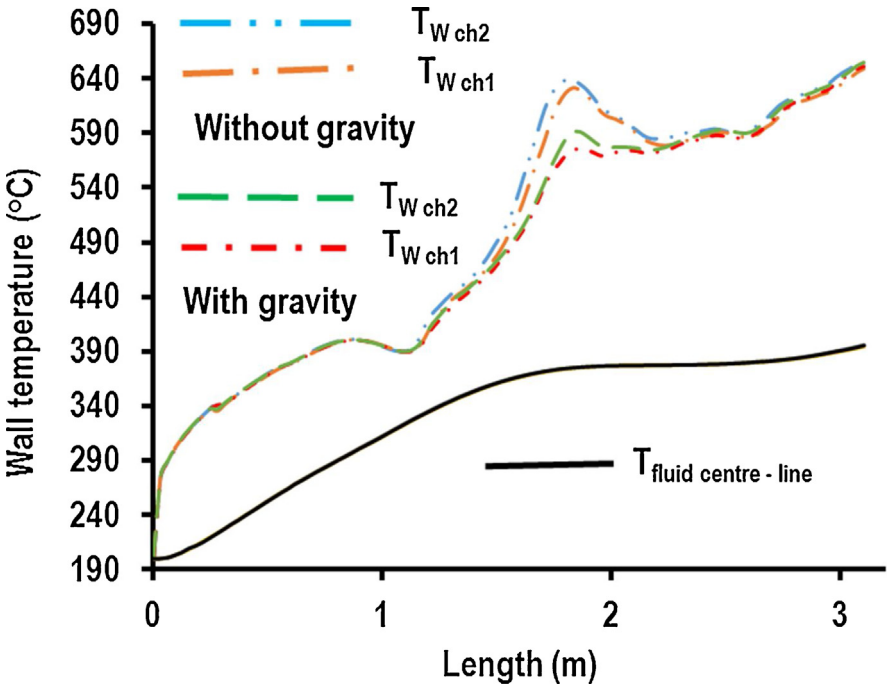

Fig. 11. Influence of gravity on HT at 23 MPa.

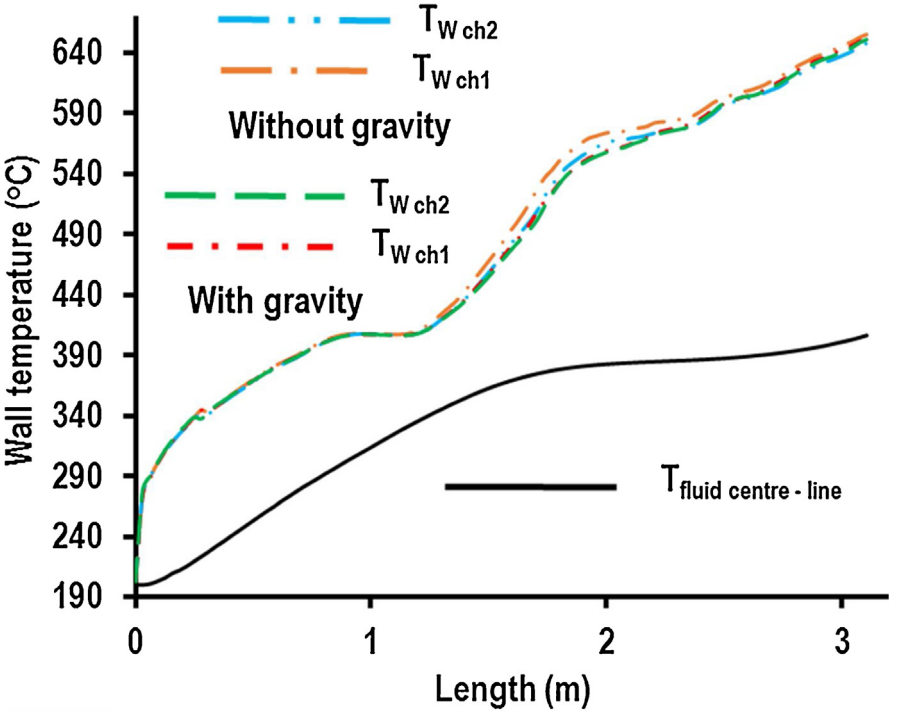

Fig. 12. Influence of gravity on HT at 25 MPa.

http://dx.doi.org/10.1016/j.heliyon.2017.e00453

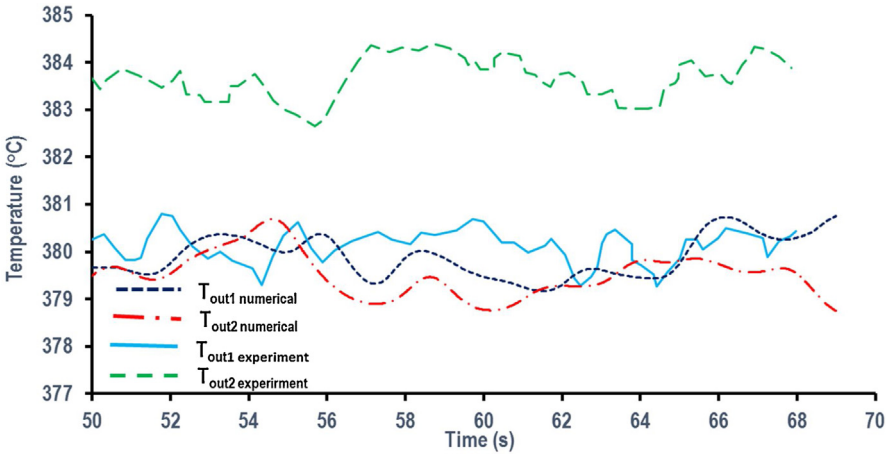

Fig. 13. Outlet temperature oscillation of each channel, Numerical and experiment. From Shitsi et al., 2017, with permission from Elsevier.

channels were compared. Fig. 13 compares results of the numerical and experimental studies of temperature oscillations at the outlet of heated parallel channels. The numerical simulation was performed at operating conditions including 190 °C coolant inlet temperature, 125 kg/h mass flow rate and 23 MPa system pressure (Xi et al., 2014a). The maximum temperature obtained at each of channel 1 and channel 2 heated outlet sections is approximately 380 °C for the numerical simulation compared to experimental results of 380 °C and 384 °C respectively (Fig. 13). The amplitude and period of temperature oscillations at the outlet of heated channels were not significantly developed for both the numerical simulation and the experiment. This is because, flow instability occurred when the outlet temperature of the heated channels was closed to pseudo-critical point. The pseudo-critical point was associated with larger specific heat which turned to limit the outlet temperature oscillation. Fig. 14 compares numerical results and experimental data for operating conditions including total mass flow rate of 125 kg/h, system pressure of 23 MPa and inlet temperatures of 180–260 °C. The trends of the numerical results and experimental data agree quite well and the numerical results are within the acceptable limit of ±10% compared to the experimental data (Fig. 15) (Xi et al., 2014a). These results show that the numerical tool adopted quite well predicted the experimental results obtained at the inlet and outlet of the heated channels.

4. Conclusions

Xi (Xi et al., 2014a) carried out experimental study and investigated flow instability in parallel channels at supercritical pressures under different mass flow rates, pressures, and axial power shapes. Experimental data on flow instability at inlet of the heated channels were obtained but no heat transfer data along the axial

http://dx.doi.org/10.1016/j.heliyon.2017.e00453

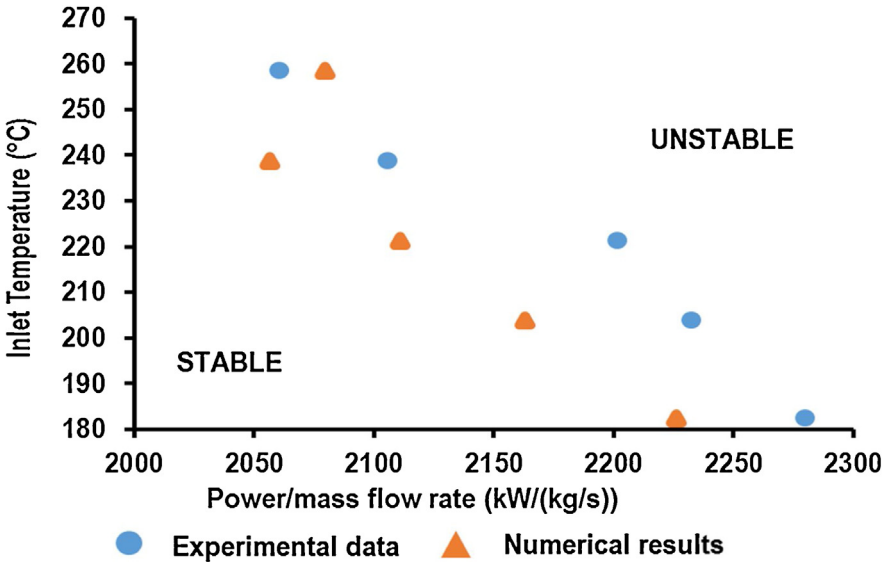

Fig. 14. Instability boundary, Numerical and experiment (P = 23 MPa, M_t = 125 kg/h). From Shitsi et al., 2017, with permission from Elsevier.

length was obtained. This numerical study used 3D numerical tool STAR-CCM+ to investigate heat transfer at supercritical pressures along the axial lengths of the parallel channels ahead of experimental data. Homogeneous axial power shape HAPS was adopted and the heating powers adopted in this work were below the experimental threshold heating powers obtained for HAPS by Xi. Inlet temperatures ranging from 180 °C to 300 °C, total heating powers ranging from

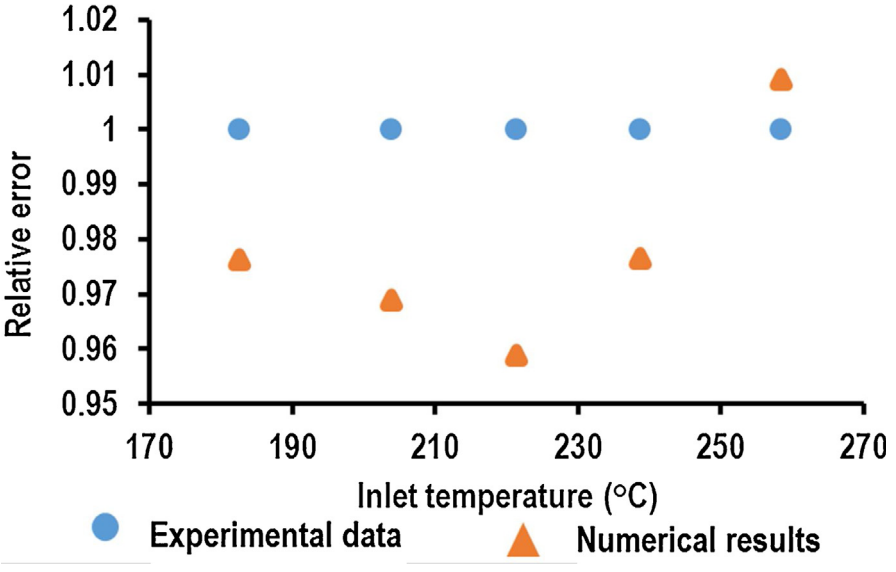

Fig. 15. Comparison between Numerical results and Experimental data. From Shitsi et al., 2017, with permission from Elsevier.

http://dx.doi.org/10.1016/j.heliyon.2017.e00453

60 kW to 72 kW, system pressures of 23 MPa and 25 MPa, and mass flow rates of 125 kg/h and 145 kg/h were the operating conditions for the numerical simulations.

Sensitivity analyses were initially performed on some selected three turbulence models TMs including LIEN, Standard k-ε and k-ω SST. The TMs tested performed better in capturing the trends for NHT, EHT and DHT regions; and also performed well in capturing the trend for recovery from DHT region. There were no significant differences in the WT values produced in the NHT and EHT regions by the three TMs at 23 MPa and 25 MPa. The significant differences in the WT values produced by the TMs occurred in the DHT region. In fact, the TMs produced nearly the same values of FCLT at both 23 MPa and 25 MPa. Since there is no available experimental data for comparing the numerical results, k-ω SST TM was selected for all the numerical simulations because it was widely reported in literature to perform better than the other TMs in most cases. The following findings were obtained from the study. The system mass flow rate, heating power, and inlet temperature have effects on FCLT below and above the PCT region, but have no effects on FCLT at the PCT region. The FCLT increased with pressure in the PCT region. The FCLT increased linearly below and above the PCT region, but flattened at the PCT region for all the operating conditions. The FCLT values in both channels 1 and 2 were nearly the same for all the operating conditions. The investigated parameters (inlet temperature, heating power, mass flow rate) have effects on WT values in the NHT, DHT and recovery from DHT regions. The WT values increased with pressure in the EHT region. The variations in the WT values in each of the heated channels 1 and 2 were not significant for change in the various operating parameters except the WT values in channel 1 were larger than that in channel 2 in the DHT and recovery from DHT regions with the increase of pressure at high mass flow rate. The numerical study was not quantitatively compared with experimental data along the axial lengths of the parallel channels, but it was observed that the numerical tool STAR-CCM+ adopted was able to capture the trends for NHT, EHT, DHT and recovery from DHT regions. The heating powers used for the various simulations were below the experimentally observed threshold heating powers for flow instability, but HTD was observed, confirming the finding that HTD could occur before the occurrence of unstable behavior at supercritical pressures (Sharabi, 2008). For purposes of comparing the results of numerical simulations with experimental data, the heat transfer data on temperature oscillations obtained at the outlet of the heated channels and instability boundary results obtained at the inlet of the heated channels were compared. The numerical results obtained quite well agree with the experimental data. This work calls for provision of experimental data on heat transfer in parallel channels at supercritical pressures for validation of similar numerical studies.

http://dx.doi.org/10.1016/j.heliyon.2017.e00453

Declarations

Author contribution statement

Edward Shitsi: Conceived and designed the experiments; Performed the experiments; Analyzed and interpreted the data; Contributed reagents, materials, analysis tools or data; Wrote the paper.

Seth Kofi Debrah: Performed the experiments; Analyzed and interpreted the data; Contributed reagents, materials, analysis tools or data.

Vincent Yao Agbodemegbe and Emmanuel Ampomah-Amoako: Performed the experiments.

Funding statement

This research did not receive any specific grant from funding agencies in the public, commercial, or not-for-profit sectors.

Competing interest statement

The authors declare no conflict of interest.

Additional information

No additional information is available for this paper.

Acknowledgements

Cd-Adapco is acknowledged for providing a reduced fee academic license and technical support in making this work possible.

References

Angelucci, M., Ambrosini, W., Forgione, N., 2013. Numerical estimation of wall friction ratio near the pseudo-critical point with CFD-models. Nucl. Eng. Des. 264, 71–79.

Cd-Adapco, 2015. User Guide STAR-CCM+ Version 10.06.009. .

Chaudri, K.S., Tian, W., Su, G., Qiu, S., 2013. Coupled neutronics/thermal hydraulics evaluation for thorium based fuels in thermal spectrum SCWR. Prog. Nucl. Energy 68, 55–64.

Cheng, X., Kuang, B., Yang, Y.H., 2007. Numerical analysis of heat transfer in supercritical water cooled flow channels. Nucl. Eng. Des. 237, 240–252.

http://dx.doi.org/10.1016/j.heliyon.2017.e00453

GIF,, 2002. A Technology Roadmap for Generation IV Nuclear Energy Systems. U.S. DOE Nuclear Energy Research Advisory Committee and the Generation IV International Forum . https://www.gen-4.org/gif/upload/docs/application/pdf/2014-03/gif-tru2014.pdf.

Gu, H.Y., Li, H.B., Hu, Z.X., Liu, D., Zhao, M., 2015a. Heat transfer to supercritical water in a 2 × 2 rod bundle. Ann. Nucl. Energy 83, 114–124.

Gu, H.Y., Hu, Z.X., Liu, D., Xiao, Y., Cheng, X., 2015b. Experimental studies on heat transfer to supercritical water in 2 × 2 rod bundle with two channels. Nucl. Eng. Des. 291, 212–223.

Gu, H.-Y., Hu, Z.-X., Liu, D., Li, H.-B., Zhao, M., Xu Cheng, X., 2016. Experimental study on heat transfer to supercritical water in 2 × 2 rod bundle with wire wraps. Exp. Therm. Fluid Sci. 70, 17–28.

Huang, D., Wu, Z., Sunden, B., Li, W., 2016. A brief review on convection heat transfer of fluids at supercritical pressures in tubes and the recent progress. Appl. Energ. 162, 494–505.

IAEA-TECDOC-1746, 2014. Heat Transfer Behaviour and Thermohydraulics Code Testing for Supercritical Water Cooled Reactors (SCWRs), IAEA TECDOC SERIES. International Atomic Energy Agency, Vienna. www-pub.iaea.org/MTCD/Publications/PDF/TE-1746_web.pdf.

Liu, L., Xiao, Z., Yan, X., Zeng, X., Huang, Y., 2013. Heat transfer deterioration to supercritical water in circular tube and annular channel. Nucl. Eng. Des. 255, 97–104.

Rahman, M.M., Dongxu, J., Beni, M.S., Hei, H.C., He, W., Zhao, J., 2016. Supercritical water heat transfer for nuclear reactor applications: A review. Ann. Nucl. Energy 97, 53–65.

NIST, 2002. Reference Fluid Thermodynamic and Transport Properties-REFPROP. In: Lemmon, E.W., McLinden, M.O., Hurber, M.L. (Eds.), NIST Standard Reference Database 23 (Software and Source) V. 7.0. U.S. Department of Commerce.

Sharabi, M.B., Ambrosini, W., He, S., 2008. Prediction of unstable behaviour in a heated channel with water at supercritical pressure by CFD models. Ann. Nucl. Energy 35, 767–782.

Sharabi, M.B., 2008. CFD Analyses of Heat Transfer and Flow Instability Phenomena Relevant to Fuel Bundles in Supercritical Water Reactors, PhD thesis presented to Dipartimento di Ingegneria Meccanica. Nucleare e della Produzione, Università di Pisa.

http://dx.doi.org/10.1016/j.heliyon.2017.e00453

Shitsi, E., Debrah, S.K., Agbodemegbe, V.Y., Ampomah-Amoako, E., 2017. Numerical investigation of flow instability in parallel channels with supercritical water. Ann. Nucl. Energy 110, 196–207.

Versteeg, H.K., Malalasekera, W., 1995. An Introduction to Computational Fluid Dynamics: The Finite Volume Method. Longman Scientific & Technical, New York. https://ekaoktariyantonugroho.files.wordpress.com/./an-introduction-to-computation.

Wang, H., Bi, Q., Wang, L., Lv, H., Leung, L.K.H., 2014. Experimental investigation of heat transfer from a 2 × 2 rod bundle to supercritical pressure water. Nucl. Eng. Des. 275, 205–218.

Wang, H., Bi, Q., Wang, L., 2016. Heat transfer characteristics of supercritical water in a 2 × 2 rod bundle - numerical simulation and experimental validation. Appl. Therm. Eng. 100, 730–743.

Wen, Q.L., Gu, H.Y., 2010. Numerical simulation of heat transfer deterioration phenomenon in supercritical water through vertical tube. Ann. Nucl. Energy 37, 1272–1280.

Xi, X., Xiao, Z., Yan, X., Li, Y., Huang, Y., 2014a. An experimental investigation of flow instability between two heated parallel channels with supercritical water. Nucl. Eng. Des. 278, 171–181.

Xi, X., Xiao, Z., Yan, X., Xiong, T., Huang, Y., 2014b. Numerical simulation of the flow instability between two heated parallel channels with supercritical water. Ann. Nucl. Energy 64, 57–66.

Yang, J., Oka, Y., Ishiwatari, Y., Liu, J., Yoo, J., 2007. Numerical investigation of heat transfer in upward flows of supercritical water in circular tubes and tight fuel rod bundles. Nucl. Eng. Des. 237, 420–430.

Zhang, S., Gu, H., Xiong, Z., Gong, S., 2014. Numerical investigation on heat transfer of supercritical fluid in a vertical 7-rod bundle. J. Supercrit. Fluids 92, 8–15.

Zhao, H., Zhu, D., Chaudri, K.S., Qiu, S., Tian, W., Su, G., 2014. Preliminary transient thermal-hydraulic analysis for new coated UN and UC fuel options in SCWR. Prog. Nucl. Energy 71, 152–159.

 http://dx.doi.org/10.1016/j.heliyon.2017.e00453